PCCP

PAPER

View Article Online
View Journal

Cite this: DOI: 10.1039/d0cp00364f

Inelastic rate coefficients based on an improved potential energy surface for $N_2 + N_2$ collisions in a wide temperature range†

Qizhen Hong, [ab] Quanhua Sun, [ab] Massimiliano Bartolomei, [c] Fernando Pirani [d] and Cecilia Coletti *[e]

Received 22nd January 2020,
Accepted 3rd April 2020

DOI: 10.1039/d0cp00364f

rsc.li/pccp

A modification in the potential energy surface (PES) for N_2–N_2 interactions, reported in the literature [D. Cappelletti *et al.*, *Phys. Chem. Chem. Phys.*, 2008, **10**, 4281], has been presented to improve its description of, particularly, the short range behavior for specific configurations, with the aim of producing a large database of vibration to vibration (V–V) and vibration to translation/rotation (V–T/R) energy transfer rate coefficients, with an increased accuracy extended to large temperature ranges relevant to the modeling of hypersonic gas flows. The modifications were introduced in a physically meaningful fashion and they are shown to improve the performance of the PES in a wide temperature range, not only for calculating rate coefficients, but also for determining a variety of physical properties. This new PES was then used to calculate V–V and V–T/R rate coefficients for inelastic N_2–N_2 collisions through a mixed quantum-classical method, based on the quantum treatment of molecular vibrations, for vibrationally excited states up to v = 40. Such a large V–T/R coefficient database is quite unprecedented, and the comparison of the efficiency of the related processes with the corresponding V–V coefficients shows that vibrational relaxation plays a very relevant role in high temperature regimes.

1 Introduction

Non-equilibrium vibrational kinetics in N_2 plasmas is of crucial importance for the correct description of discharges/post-discharges[1,2] and high-temperature phenomena involving high-speed shock waves in atmospheric entries.[3–5] In such non-equilibrium situations, the population of vibrational states usually strongly deviates from the Boltzmann distribution. Therefore if one wanted to reproduce the detailed vibrational distribution, rate coefficients of the vibration–translation/rotation (V–T/R) and vibration–vibration (V–V) energy exchange processes should be considered with a high accuracy.

However, for the V–T/R and V–V transitions occurring in N_2, the experimental determinations are difficult because N_2 does not exhibit a permanent dipole moment and the number of processes to be described for a reasonable modeling of non-equilibrium kinetics in a wide temperature range would require the selection of a variety of initially vibrationally excited states, therefore the relevant rate coefficients remain rather scarce. As a result, most such rates, especially of $N_2 + N_2$ collisions, are based on numerical scattering calculations by using quasi-classical[6–10] and mixed quantum-classical methods.[11–13] The latter, including the most relevant quantum effects in the dynamics, are often required to get the correct behavior at low temperatures (where vibrations and, in some cases, rotations show a quantum behavior), but they also provide a better description of multi-quantum energy exchange processes which might have large probabilities at high temperatures.[14,15]

The accuracy of the rate coefficient, obtained by calculations, depends on the reliability of the formulation of the inter-molecular interaction which drives the collisions. In particular, most appropriate conditions are reached when the formulation is accurate in the full space of relative configurations and the separation distances of the involved partners. Indeed, though high temperature dynamics is mainly governed by short range interactions and the long range potential plays a crucial role in the description of low temperature processes, non-negligible effects often arise from the interplay of the different contributions to the full interaction potential. This is why the correct modeling of

[a] *State Key Laboratory of High Temperature Gas Dynamics, Institute of Mechanics, Chinese Academy of Sciences, 100190 Beijing, China*
[b] *School of Engineering Science, University of Chinese Academy of Sciences, Beijing 100049, China*
[c] *Instituto de Física Fundamental – CSIC, C/Serrano 123, Madrid, Spain*
[d] *Dipartimento di Chimica, Biologia e Biotecnologie, Università di Perugia, via Elce di Sotto, 8 – 06183 Perugia, Italy*
[e] *Dipartimento di Farmacia, Universitá G. d'Annunzio Chieti-Pescara, via dei Vestini, I-66100 Chieti, Italy. E-mail: ccoletti@unich.it*

† Electronic supplementary information (ESI) available: Tables and figures indicated in the paper and the subroutine with the new potential energy surface for $N_2 + N_2$. See DOI: 10.1039/d0cp00364f

every dynamical process in the full range of temperature requires the knowledge of a potential energy surface (PES) which should be able to accurately describe both long-range and short-range interactions. Potentials which work well for the description of specific phenomena are not bound to perform equally well for processes driven by the different regions of the interaction field. Besides, specific reciprocal orientations of the colliding diatoms might have a larger effect on the outcome of the process.

Analytical PESs exploiting the partitioning of the interaction according to different contributions (exchange-repulsion, electrostatic, induction and dispersion components) are often used for the calculation of V–T/R and V–V rates. Such PESs adopt a formulation based on experimental or semiempirical parameters[16,17] and they were found to give a good description at high and medium temperatures ($T > 1000$ K) for V–T/R coefficients. Furthermore, due to the relevance of N_2–N_2 interactions for the modeling of transport properties, and thermophysical properties, *etc.* in nitrogen, quite a number of *ab initio* potentials have been developed over the years, with different performances in the calculation of different phenomena.[18,19] Recently, a potential energy surface for $N_2 + N_2$ collisions[7,20] which includes possible reactive channels was also developed, based on CASPT2/maug-cc-pVTZ *ab initio* points to model the very high temperature regime where highly excited vibrational states are populated and multiple reaction channels are open. However, first attempts to use this PES for the description of inelastic scattering at a temperature less than 5000 K produced poor results.[8,11] The reason for such a failure is probably associated with the fact that the description of inelastic scattering phenomena requires a potential energy surface correctly describing, for all possible configurations, large diatom-diatom interaction distances (up to several tens of Angstroms), the potential wells and the first repulsive walls. At present, *ab initio*-based potentials are not in general suitable, since they would require the determination of a very large number of points, in order to systematically cover all the desired regions.

The early motivation for the present work arises from the need for a wealth of V–V (including the often neglected rates for multiquantum transitions) and, above all, V–T/R rates, which are usually less available due to the large computational effort required for their calculation, in a large temperature range, useful for the modeling of hypersonic flows based on a reliable potential energy surface. To achieve this aim we chose the PES derived in ref. 16 which was shown to produce a fairly good agreement with experimental values for the derivation of V–V processes in the low-medium temperature range[11,12] and to reproduce accurately the second virial coefficient and total cross section data, available from molecular beam scattering experiments. Such a PES was also compared with previously calculated *ab initio* energies.[21]

Furthermore, the formulation of such potential has several advantages, arising from the fact that it is completely general, that each term is physically meaningful, the parameters can be modulated in a flexible fashion and that the contribution to the van der Waals component of the interaction (defined as size repulsion plus dispersion attraction) of different configurations, *i.e.* different reciprocal orientations of the diatoms, is accounted for separetely. This makes such a formulation a powerful tool to get physical insights into the nature of the interaction, as well as into the understanding of the anisotropy and orientation effects that often determine the evolution of the collisional phenomena, particularly at low temperature.

The mixed quantum-classical (traditionally called semiclassical in many previous applications) method developed by Billing[22,23] for the treatment of inelastic scattering (also for rotational energy transfer[24,25]) was therefore used here in the formulation reported in ref. 14 and 26, where vibrations are treated in a quantum mechanical framework, to calculate V–V and V–T/R rate coefficients over a wide range of temperature and compared to the available experimental ones. This analysis, together with a stringent comparison to new high level *ab initio* energy values, led us to propose an improvement in the existing PES, particularly in the short range region and for collinear collisions, conditions which appear to be relevant to vibrational energy exchange at very high temperatures.

This PES was thus used to build a large database (which is also meant to complete available ones[27]), extending available V–V to achieve higher vibrational states and a larger range of temperature and multiquantum transitions. Furthermore, we focus on the calculation of V–T/R rate coefficients, which are not included in existing databases with the exception of $N_2(1) + N_2(0)$ collisions, and on their role under high temperature conditions, relevant to the modeling of plasmas and hypersonic flows.

The paper is therefore organized as follows. Section 2 is devoted to briefly describing the main features of the quantum-classical method. In Section 3, the formulation of the $N_2 + N_2$ PES, its comparison against experimental and *ab initio* data and its subsequent improvement have been described. Section 4 reports the qualitative and quantitative features of the database obtained with the improved PES. Concluding remarks are given in Section 5.

2 The quantum-classical method

This approach was introduced and developed by G. D. Billing[22,23] and is proven to be accurate and efficient in the calculation of large bodies of rate constants for processes involving vibrational energy transfer. The simplifying assumptions made in this method are a classical treatment of the translational and rotational motion of both molecules. Thus, only the vibrational degrees of freedom are quantized. Further theoretical foundations of the method will be sketched in the following sections; for more information, readers are refered to ref. 22 and 23.

According to the spirit of the quantum-classical method, vibrations and roto-vibrational couplings are treated quantum-mechanically using close coupled equations. In order to obtain the amplitudes $a_{v_1'v_2'}$ for the process $N_2(v_1) + N_2(v_2) \rightarrow N_2(v_1') + N_2(v_2')$, we first expand the quantum vibrational wavefunction (perturbed by the rotational distortion at the first order) in terms of the product of Morse wave functions $\phi_{v_1}\phi_{v_2}$ of the two unperturbed oscillators:

$$\Psi = \sum_{v_1 v_2} a_{v_1 v_2}(t)\phi_{v_1}\phi_{v_2} \exp\left[-\frac{it\left(E_{v_1} + E_{v_2}\right)}{\hbar}\right], \qquad (1)$$

where E_v is the anharmonic vibrational energy, which is approximated as

$$E_v = \hbar\omega_e\left(v+\frac{1}{2}\right) - \hbar\omega_e x_e\left(v+\frac{1}{2}\right)^2 + \hbar\omega_e y_e\left(v+\frac{1}{2}\right)^3, \quad (2)$$

where ω_e is the wavenumber for the oscillator and x_e and y_e are the anharmonicity constants. Then one can obtain from the time-dependent Schrödinger equation the following set of coupled equations for the amplitudes:

$$i\hbar\dot{a}_{v_1'v_2'}(t) = \sum_{v_1v_2}\left[\left\langle\phi_{v_1'}\phi_{v_2'}\middle|V(r_1,r_2,t) + i\hbar H_{C_0}\middle|\phi_{v_1}\phi_{v_2}\right\rangle\right] \cdot a_{v_1v_2}(t)\exp\left[\frac{i}{\hbar}\left(E_{v_1'} + E_{v_2'} - E_{v_1} - E_{v_2}\right)t\right], \quad (3)$$

where the matrix elements $\langle\ \rangle$ of the potential V are obtained by integrating over the oscillator distances r_1 and r_2. The H_{Co} term is the rotational distortion due to the Coriolis centrifugal stretch, which depends on the rotational angular momenta of the two molecules.[22]

On the other hand, the translational and rotational motions are obtained by solving the corresponding Hamilton equations by making use of an Ehrenfest averaged potential[28] defined as the quantum expectation value of the interaction potential. Lagrange multipliers are introduced in the Hamiltonian to keep the two oscillator distances fixed at their equilibrium values r_e (details can be found in ref. 22 and 28). Note that the intramolecular potential depending on the actual values of the diatomic distance is used in the quantum mechanical subsystem. A variable-order variable-step Adams predictor-corrector integrator,[29] is then used to solve the coupled equations (eqn (3)) and the classical equations of motion for rotations and translations. An absolute integration accuracy of 10^{-8} is achieved for all calculations in this work, by using an initial time step of 0.1×10^{-14} s and an initial integration order of 1. Both of them, however, are automatically varied to reach the desired accuracy.

The vibrational wavefunction is initialized as the product of the Morse functions for the two infinitely separated diatoms. The simultaneous propagation of the quantum and classical sets of equations produces the quantum transition amplitudes $a_{v_1'v_2'}$ which can be used to calculate cross sections for the vibrational transitions. The cross sections are obtained by averaging over a number of trajectories under randomly selected initial conditions, and a Monte Carlo average over the initial Boltzmann distribution of rotational energy is generally introduced to have rate coefficients for vibrational relaxation. Thus, an averaged cross section is defined as:

$$\sigma_{v_1v_2\to v_1'v_2'}(U,T_0) = \frac{\pi\hbar^6}{8\mu k_B{}^3T_0{}^3I_1I_2}\int_0^{l_{max}}\int_0^{j_{1max}}\int_0^{j_{2max}} dj_1dj_2dl \times (2j_1+1)(2j_2+1)(2l+1)P_{v_1v_2\to v_1'v_2'}, \quad (4)$$

where μ is the reduced mass for the relative motion, l is the orbital and j_i is the rotational angular momentum of molecule i. The moment of inertia is $I_i = m_ir_i^2$ and the temperature T_0 is arbitrary because it is cancelled out when calculating the rate coefficient. j_{1max} and j_{2max} are the upper limit for the randomly chosen rotational quantum numbers for the diatoms and l_{max} is the upper limit for the angular momentum. Rate coefficients are then calculated using the following equation

$$k_{v_1v_2\to v_1'v_2'}(T) = \left(\frac{8k_BT}{\pi\mu}\right)^{1/2}\left(\frac{T_0}{T}\right)^3\int_0^\infty d\left(\frac{\bar{U}}{k_BT}\right) \cdot\exp\left(-\frac{\bar{U}}{k_BT}\right)\sigma_{v_1v_2\to v_1'v_2'}(T_0,\bar{U}), \quad (5)$$

which only holds true for exothermic processes. $\bar{U}$ is the symmetrized classical energy, which should be introduced to restore the detailed balance principle.[22,28]

With the aim to compare V–V,

$$N_2(1) + N_2(0) \rightarrow N_2(0) + N_2(1),$$

and V-T/R,

$$N_2(1) + N_2(0) \rightarrow N_2(0) + N_2(0),$$

rate coefficients calculated with the original PES[16] and its modifications (see the following description) and the experimental data, our investigation was carried out over a wide range of temperatures by running trajectories at 35 initial values of total classical energy comprised between 35 cm^{-1} and 80 000 cm^{-1}, with a more frequent sampling directed towards lower energies. For each energy value, 2000 trajectories were considered, which should ensure an accuracy for rate constants of *ca.* 20% at low temperatures and *ca.* 10% at high temperatures. An initial separation of the diatoms equal to 15 Å for the V–V energy transfer and 80 Å for the V–T/R energy transfer, and an impact parameter randomly chosen between 0 and 9 Å were utilized. For these processes 24 initial vibrational states were considered in a set of coupled time dependent quantum equations to be solved for the vibrational motion.

3 Potential energy surface

The formulation of the PES is essentially the same as those reported in ref. 11, 12 and 16, which will be briefly described in the following sections.

The overall interaction V of the diatom–diatom system is as usual expressed as a sum of intramolecular (V_{intra}) and intermolecular (V_{inter}) interaction components. To be more specific, V_{intra} is formulated using a Morse potential energy function $D_e(t^2 - 2t)$, in which D_e is the dissociation energy of the diatomic molecule, $t = \exp[-\beta(r - r_e)]$ and r is the real internuclear diatomic distance (with r_e being its equilibrium value). A set of Morse parameters derived from spectroscopic data reported in ref. 30 is shown in Table 1. This set of parameters is also used to define the Morse function in the quantum-classical calculation.

The intermolecular (V_{inter}) interaction component is represented as the sum of two main contributions:

$$V_{inter} = V_{vdW} + V_{elect}, \quad (6)$$

where the V_{vdW} term accounts indirectly for three body effects, being formulated in terms of a bond–bond interaction.[16] The

Table 1 Molecular constants for N_2[30]

ω_e	2359.60 cm^{-1}
x_e	0.006126
y_e	0.0000032
r_e	1.098 Å
β_e	2.689 Å^{-1}
D_e	9.905 eV
Q_e	−1.1 a.u.

V_{elect} term accounts for the electrostatic interaction due to the molecular permanent multipoles and only the main quadrupole–quadrupole term is taken into account herein as reported in the literature.[11,16,17]

The V_{vdW} interaction depends on the distance R between the centers of mass of the interacting partners, and on θ_a, θ_b, Φ, the four body Jacobi angular coordinates which describe the relative orientation of the two diatoms.

Specifically, the parametrization adopted for the V_{vdW} pair potentials (size repulsion plus dispersion attraction) is as follows:[31,32]

$$V_{vdW}(R,\gamma) = \varepsilon(\gamma)\frac{6}{n(R,\gamma)-6}\left(\frac{R_m(\gamma)}{R}\right)^{n(R,\gamma)} - \varepsilon(\gamma)\frac{n(R,\gamma)}{n(R,\gamma)-6}\left(\frac{R_m(\gamma)}{R}\right)^{6}, \quad (7)$$

where $\gamma = (\theta_a,\theta_b,\Phi)$ and ε and R_m are the bond–bond interaction well depth and its location, respectively. This function gives a more realistic representation of both the repulsion and the long range attraction compared to the classic Lennard-Jones potential.[33] The n term is expressed as a function of both R and γ:

$$n(R,\gamma) = \beta + 4.0\left(\frac{R}{R_m(\gamma)}\right)^2, \quad (8)$$

where β is a parameter which depends on the hardness of the interacting particles. β has been fixed here to 10,[16] a value suitable for neutral–neutral interactions.

The angular dependence of the V_{vdW} term is obtained by representing the potential parameters ε and R_m in a spherical harmonic expansion. In this way, the reduced form of the V_{vdW} potential is taken to be the same for all orientations, as stressed in ref. 16 and 34. The detailed representations of ε and R_m are those originally reported in ref. 16 and the utilized values are listed in Table 2.

Table 2 Parameters for the N_2–N_2 intermolecular potentials. The R_m (Å) and ε (meV) values define the vdW components in the relevant configurations of the complexes, defined by the θ_a, θ_b and Φ angles (in degrees), and the corresponding monomers at the equilibrium bond length, r_e

		Original PES		Modified PES	
Configuration (i)	(θ_a,θ_b,Φ)	R_m^i	ε^i	R_m^i	ε^i
H	(90,90,0)	3.73	12.5	3.73	12.5
X	(90,90,90)	3.73	12.5	3.73	12.5
T	(90,0,0)	4.11	9.38	4.11	9.38
I	(0,0,0)	4.55	6.40	4.82	5.64

The V_{elect} term of eqn (6) is given by

$$V_{elect}(R,\gamma) = \frac{Q_a Q_b}{R^5}A^{224}(\gamma) \quad (9)$$

where Q_a and Q_b (Q in Table 1) correspond to the quadrupole moments of the monomers[35] and $A^{224}(\gamma)$ is the bipolar spherical harmonic which describes the angular dependence of the quadrupole–quadrupole interaction.

Note that both V_{vdW} and V_{elect} intermolecular components include the dependence on monomer deformations by exploiting the bond length dependence of N_2 polarizability and quadrupole moment (see Appendix B of ref. 16).

The extrapolation of the rigid rotor PES, in order to include the dependence on flexible monomers, has been considered and previously described in ref. 16: in particular, this is implicitly introduced by considering the N_2 bond length dependence of both molecular polarizability and quadrupole moment. In order to explicitly test the validity of this approach, in the present paper we have performed further *ab initio* calculations of the intermolecular interaction with both monomers stretched by 10% and 20% (with respect to equilibrium distance) and the results are reported in Fig. S1 of the ESI.† From the comparison between the predicted and *ab initio* results, it can be appreciated that the trends of the potential energy curves, corresponding to the dimer limiting configurations, provided by the present semiempirical formulation of the multidimensional PES and calculated *ab initio*, are consistent. Accordingly, for slight and moderate monomer deformations the reliability of the results provided by the present formulation of the interaction has been directly proved. Moreover, since the variation of the quadrupole moment of N_2 and the variation of its parallel and perpendicular polarizability components, adopted to predict the change of the potential parameters, agree with theoretical values in a wider range of molecular deformation,[36] we are confident that the proposed formulation is reliable up to the molecular deformation of 30–40%, a requirement necessary to represent the behavior of highly vibrationally excited molecules.

As mentioned in the previous section, a set of preliminary calculations was carried out to investigate the ability of the original potential to accurately determine V–T/R and V–V rates in a wide temperature range. Experimental data are indeed available for V–T/R $N_2(1) + N_2(0) \rightarrow N_2(0) + N_2(0)$ (hereafter indicated as (1, 0) → (0, 0) in short) and V–V $N_2(1) + N_2(0) \rightarrow N_2(0) + N_2(1)$ (hereafter indicated as (1, 0) → (0, 1)) processes allowing to test the performance of this PES.

V–T/R rate coefficients calculated with this PES (dash–dotted black lines in Fig. 1) present a reasonable qualitative agreement with experimental data of ref. 37 at high and medium temperatures (whose uncertainties are of ±15%), and of ref. 38 and 39 at a low temperature; however they tend to quantitatively underestimate the experimental values, (see also Table S1, ESI†). Results using other recent previous analytical PESs[12] show the same tendency to underestimate experimental values in the low temperature regime.

For the V–V (1, 0) → (0, 1) resonant exchange, a series of experimental data are available at 300 K ranging from 0.90×10^{-14} [40] to 9.93×10^{-14} [41] together with those of a recent

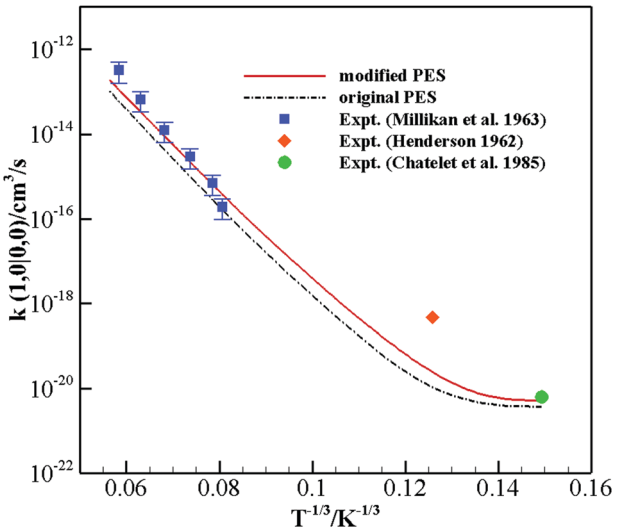

Fig. 1 Landau–Teller plot of the rate coefficients for the transition (1, 0) → (0, 0) calculated on the original PES (dash–dotted black lines) and the modified PES (full red lines). Experimental data of ref. 37 (blue squares), ref. 38 (red diamonds) and ref. 39 (green circles) have also been reported.

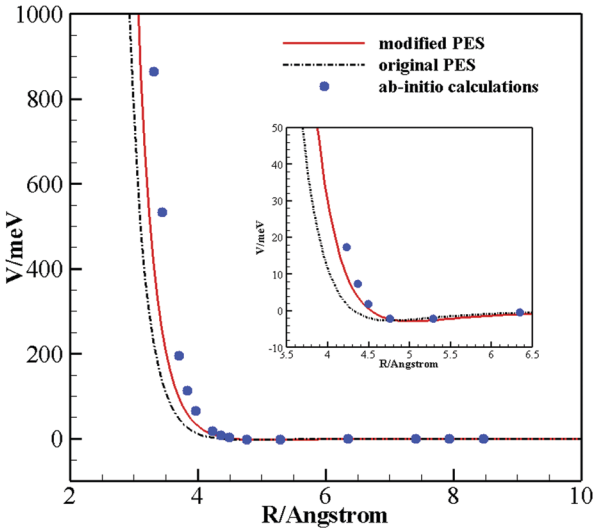

Fig. 3 Behavior of the original and modified potential energy surfaces as a function of the intermolecular distance in the I configuration.

study[42] in the low temperature regime (77–300 K), see Table S2 (ESI†). V–V rates based on this PES (dash–dotted black lines in Fig. 2) fall within the range of experimental determination at 300 K and show the correct qualitative behavior (including the inversion of the temperature dependence at low T values), but again tend to underestimate the quantitative results.

Because the high temperature regime is essential to model hypersonic flows and since the nature of the formulation of the present PES allows us to investigate the physical motivations of such behavior (*i.e.* the contributions coming from different interaction regions or different configurations), we considered the possibility of changing some of the parameters to improve its behavior for the description of inelastic scattering.

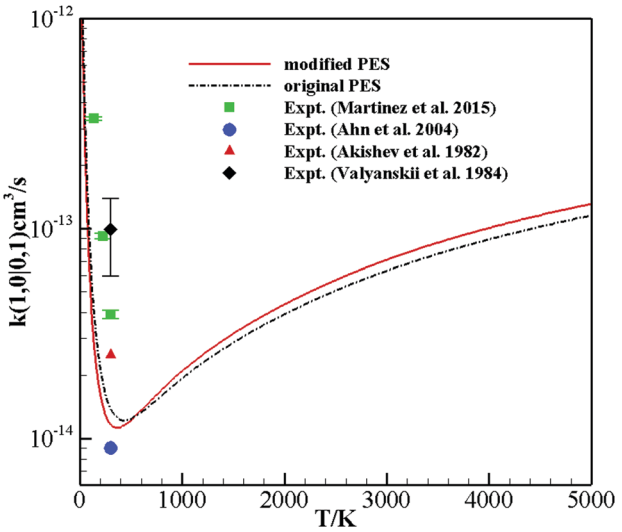

Fig. 2 Rate coefficients as a function of temperature for the (1, 0) → (0, 1) transition calculated on the original PES (dash–dotted black lines) and the modified PES (full red lines). Experimental data of ref. 40 (blue circles), ref. 41 (black diamonds), ref. 42 (green squares) and ref. 43 (red triangles) are also reported.

In order to do that in a physically meaningful fashion, significant sections of the PES were compared to the corresponding supermolecular *ab initio* energies, focusing in the short range and well regions. Such sections, representing the potential energy as a function of the centers of mass (intermolecular) distance R of the diatoms at their equilibrium geometry, are reported in Fig. 3 for the collinear (or I) configuration and in Fig. S2 of the ESI,† for the parallel (or H), the perpendicular (or T) and the crossed (or X) configurations. For all N_2–N_2 supermolecular *ab initio* calculations, the CCSD(T) level of theory was used together with Dunning's aug-cc-pVQZ basis set[44] and the bond function set [3s3p2d1f] developed by Tao[45] and placed at the midpoint of the intermolecular distance R. The obtained interaction energies were corrected using the counterpoise method[46] in order to remove the basis set superposition error and all computations were performed by using the Molpro code.[47]

The comparison shows that this PES gives an excellent description at long range in all cases, and the interaction potential well shows very good agreement for the X and T configurations, while showing some small discrepancies for the collinear I configuration. The very short range part is also well described for the T configuration, while for the I one it is less repulsive than the *ab initio* points whereas the opposite behavior (a too repulsive wall) is shown for the X configuration. Because the results in Fig. 1 and 2 show a general tendency to underestimate experimental values, particularly at high temperature, a manifestation of an incorrect behavior mostly at short range, we decided that improvements should involve the collinear configuration in the first place, which shows the largest differences with *ab initio* energy values in such a region. Besides, this specific orientation of the interacting diatoms can be easily thought to be the most effective for the exchange of vibrational quanta of energy, so that its modeling is crucial to correctly deal with inelastic scattering phenomena.

For this reason, the values of R_m and ε corresponding to the collinear configurations were increased by 6% and decreased by 13%, respectively (see Table 2). Such a change is expected to produce a shift at a larger distance of the repulsive wall associated with this configuration, that can favor the overlap of the vibrational wavefunctions and promote the exchange of the vibrational quanta between the diatoms.

The behavior of the modified PES for the I configuration (Fig. 3, red solid lines) shows indeed an improvement: the well is now reproduced in an excellent fashion and the short range wall is more repulsive. There is no change in the other configurations, whose energy values as a function of R were already very close to the *ab initio* points.

A more extensive comparison of the behavior of the present PES with some of the existing semiempirical or *ab initio* potentials is shown in Fig. 4 for all configurations. In particular, the figure shows the *ab initio* PES reported in ref. 21 based on CCSD(T) *ab initio* points calculated with a basis set of triple-ζ quality (*ab initio* 2007), the recent reactive *ab initio* PES reported in ref. 7 (UMN), the analytical semiempirical PES (called PES0 in ref. 12) on which a large database of quantum-classical V–V rates was constructed.[27] The UMN PES, though accurately representing short range and (in its most recent version) long range asymptotic behavior, is not able to describe the shallow interaction minima, confirming its usefulness only in the very high temperature regime, mainly driven by the very short range part of the potential.

For the linear configuration I, the most relevant for the exchange of vibrational quanta of energy, the well region is accurately represented only by the newly modified PES, with PES0 and the *ab initio* 2007 PES showing a slightly too deep well. This is also true, even if up to a lesser extent, for T and H configurations, whereas for the H configuration the *ab initio* 2007 PES gives a closer agreement with the *ab initio* points. In this case too, however, the asymptotic behavior of the present PES up to the minimum is identical to the *ab initio* points and the *ab initio* 2007 PES. This comparison thus shows an overall very good performance of the presently modified PES for all configurations and all ranges (which is not the case for previous PESs which perform differently according to the investigated region or configuration) with discrepancies only arising in the very repulsive region.

The modified PES (available in the ESI†) was thus used to calculate again V–T/R and V–V rate coefficients (Fig. 1 and 2, respectively, red solid lines and Tables S1 and S2 (ESI†), respectively, and Fig. S3, ESI†). Calculated values for the V–T/R (1, 0) → (0, 0) process now show an excellent agreement with

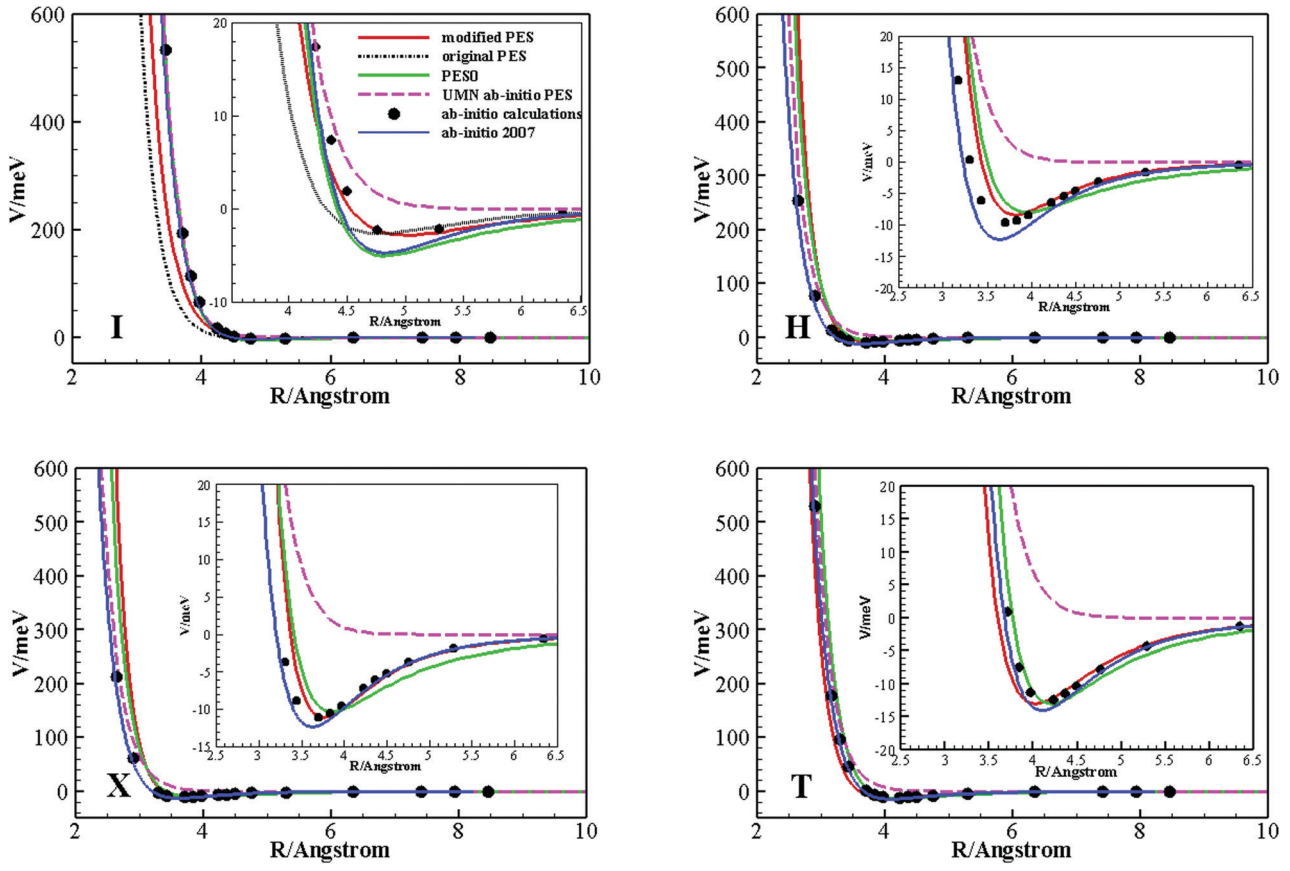

Fig. 4 Behavior of different potential energy surfaces as a function of the intermolecular distance. Selected configurations, at the equilibrium intramolecular distance of both monomers, are considered: diatoms approaching in a collinear configuration I ($D_{\infty h}$ symmetry, panel I), in a parallel fashion (H configuration, D_{2h} symmetry, panel H); in a crossed X fashion (D_{2d} symmetry, panel X) and perpendicularly, according to a T orientation (C_{2v} symmetry, panel T).

the experimental data both at high and low temperatures, whereas for the V–V rate coefficients no substantial differences can be seen in comparison with the experimental data. However, such values are available only at a low temperature and modifications on the short range potential are not expected to make relevant changes in the description of such regimes. On the other hand the modified PES shows larger V–V values than the original ones at high temperature. The still existing differences at very low temperatures with the experimental results might also be due to the fact that rotations are needed to be included in the quantum treatment under such conditions. Moreover, at small collision energies, symmetry issues, including the population of ortho and para states might play a crucial role[48] and thus the corresponding collisions might need a separate treatment.

3.1 Test of the modified PES on other experimental findings

Together with the improved performance of the modified PES to calculate rate coefficients relevant to inelastic scattering events, we would like this PES to reproduce well other experimental quantities corresponding to different physical processes which might be governed by different interaction regions.

In ref. 16, for instance, it was shown that the original PES provided very good results for the calculation of the second virial coefficient, $B(T)$, values, including first quantum correction $B_{ql}(T)$ to the classical estimate $B_{cl}(T)$[49] ($B(T) = B_{ql}(T) + B_{cl}(T)$). The same calculation carried out with the modified PES leads to even better results in comparison with the experimental measurements[50] than the original one (Table 3, where comparison with the results obtained by the *ab initio* 2007 PES[21] is also reported). This is especially true for values of $B(T)$ at medium and high temperatures ($T > 125$ K) where differences with the experimental values are generally well below 5%. It is indeed known that negative second virial coefficient values, at low T, mostly depend on the interaction anisotropy in the attractive part of the PES, while at high T (positive values) they probe the first repulsive region of the same PES. Thus, a more correct behavior of the modified PES in the short range repulsive region not only leads to a sensible improvement in reproducing experimental data at high T, but the now more accurate description of the interaction

Table 3 Calculated and experimental second virial coefficient $B(T)$ (in cm^3 mol^{-1} units) as a function of temperature

T (K)	*Ab initio*[21]	Original PES	Modified PES	Experiment[50]
75.0	−344.08650	−275.41810	−275.81770	−276.10000
80.0	−303.07648	−243.54484	−243.89335	−243.90000
90.0	−241.68422	−195.15992	−195.39894	−195.00000
100.0	−198.10613	−160.27300	−160.40574	−159.80000
110.0	−165.68083	−133.99149	−134.02712	−133.30000
125.0	−130.20387	−104.89316	−104.80265	−104.00000
150.0	−91.38226	−72.60684	−72.35189	−71.50000
200.0	−49.03708	−36.81831	−36.35037	−35.60000
250.0	−26.61535	−17.61612	−17.02208	−16.30000
300.0	−12.86470	−5.75467	−5.08026	−4.50000
400.0	2.91967	7.93400	8.70015	9.20000
500.0	11.54387	15.43949	16.25237	16.60000
600.0	16.85949	20.07059	20.90880	21.10000
700.0	20.39045	23.14655	23.99862	24.10000

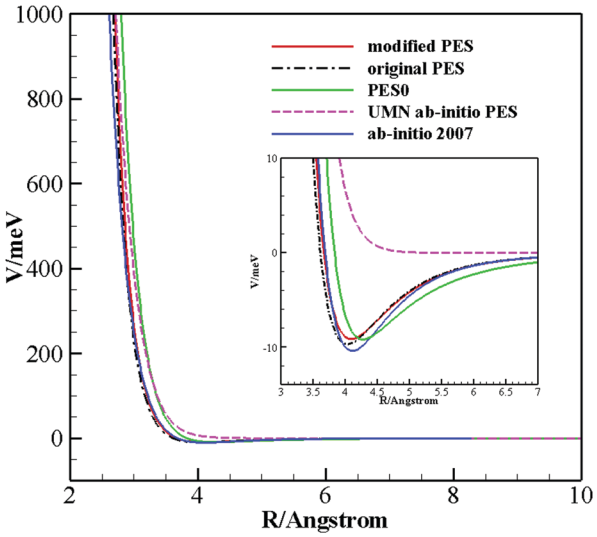

Fig. 5 Spherical average of different potential energy surfaces as a function of the diatomic interaction distance.

well in the I configuration also produces an improvement for the negative second virial coefficients starting from temperatures above 125 K.

The total scattering cross sections have been measured using the molecular beam technique in a wide collision velocity range and under high angular and velocity resolution conditions, proper to resolve quantum interference ("Glory" effect) in the scattering. It is well known[31] that while the average component of cross sections is directly related to the average attraction in the long range, the glory pattern depends on the value of the interaction and on its anisotropy in the potential well region. In particular, while position and frequency of the oscillations arise from the isotropic component of the PES, their amplitude varies with the anisotropy. The modified PES shows an isotropic component consistent with that of the original one (Fig. 5), whereas its slightly increased anisotropy should provide a more efficient glory quenching at high velocity, in agreement with the experimental results.

Moreover the modified PES gives a value for the C_6 coefficient, which describes the average dispersion in the long range, obtained as the asymptotic value of the ILJ function, equal to 71 a.u. (*vs.* 69 a.u. obtained with the original PES), in excellent agreement with the values of 73.22 a.u. proposed by Olney *et al.*[51] from both experimental measurements and *ab initio* calculations on the induced dipole–induced dipole interaction and the ab intio one of 73.47 a.u. reported in ref. 35.

Therefore, experimental findings of quite a different type, probing complementary aspects of the interaction, are all very well reproduced by the present PES, which is thus demonstrated to be a tool for the simulation of properties of the N_2 + N_2 system, beyond V–V and V–T/R rate coefficients.

4 Results and discussion

The improvement in the reproduction of experimental data of different sources shows that the modified PES can be safely

used to calculate many kinds of properties. Therefore, we used the present PES to build a large database for V–V and V–T/R rate coefficients to extend and complete existing sources for the investigated system.

Indeed a large database, based on a similar quantum-classical method and on the potential here indicated as PES0, is already available,[27] focusing on V–V transitions for temperature values up to 2900 K, including single-, double- and some multi-quantum transitions.

The present database, besides enlarging the number of the considered V–V transitions and the considered range of temperature values (20–7000 K), also includes V–T/R single and multiquantum energy exchange, for a wide range of initial vibrationally excited states. The determination of such rate coefficients, more sensitive to long range interactions, requires large initial intermolecular distances and thus a large computational effort, so that they are very seldom calculated and, to the best of our knowledge, they are not included in any previous database.

V–V rate coefficients involving highly excited vibrational states were calculated here by coupling 81 initial vibrational states while the other calculation specifications are the same as for the (1, 0) → (0, 1) calculations (*i.e.* by starting from an initial diatom separation distance equal to 15 Å and 35 different values of total classical energies, comprised between 35 cm^{-1} and 80 000 cm^{-1}). For the calculation of V–T/R rate coefficients, the same specifications as for the (1, 0) → (0, 0) calculations were considered, but coupling, in this case, 81 vibrational states for $10 \leq v \leq 30$ and 121 states for $v > 30$.

From the somewhat smaller accuracy in the PES for very elongated intramolecular distances, and from the fact that the Morse potential and Morse wavefunctions are less accurate when describing highly vibrational excited states, rate coefficients pertaining to processes involving vibrational states with $v \geq 35$ are bound to have a global uncertainty larger than the above mentioned 20%. However, we still believe them to give a reasonable estimate (and certainly to be more accurate than those available through extrapolation procedures or by using first order treatments) for such processes and to provide the correct qualitative trend in their variation. Yet, their value should be read with some caution.

Table 4 reports a comparison between the values of rate coefficients calculated with the present PES and those reported in the database of ref. 27 for symmetric single quantum and asymmetric multiquantum vibrational energy exchange. It might be noted that the present values are about a factor of two smaller, which could be due to the too attractive well and the larger repulsive wall in PES0. This trend is constant in the whole range of temperature evaluated in that investigation.

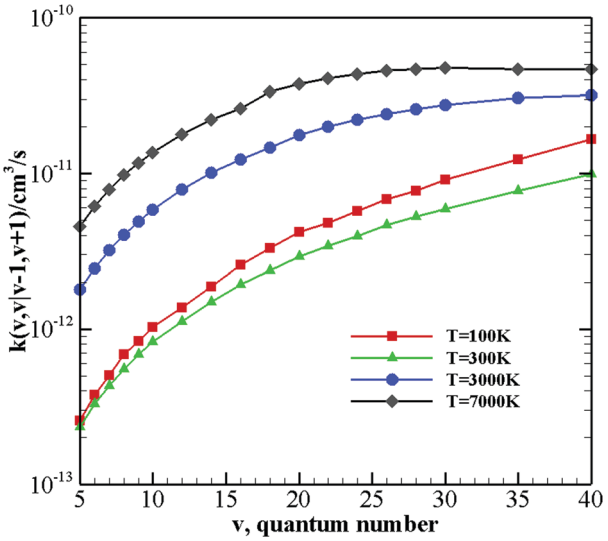

Fig. 6 V–V rate coefficients for $N_2(v) + N_2(v) \rightarrow N_2(v-1) + N_2(v+1)$ processes as a function of the vibrational quantum number v at different temperature values.

Tables listing rate coefficients for single quantum symmetric (Table S3, ESI†), symmetric multiquantum (Table S4, ESI†), and asymmetric multiquantum V–V transitions (Table S5, ESI†), obtained through the present study, are reported in the ESI.†

Fig. 6 shows the calculated V–V rate coefficients for $N_2(v) + N_2(v) \rightarrow N_2(v-1) + N_2(v+1)$ processes as a function of the vibrational quantum number v at 100 K, 300 K, 3000 K, and 7000 K. An anti-Arrhenius behavior of the rate coefficients, *i.e.* the decrease of the rate coefficients with temperature in the low temperature regime, is shown for all initial v values, and in fact this tendency slightly grows with increasing v. This is shown in Fig. S4 in the ESI,† where $\ln k$ is reported as a function of $1/T$ for some selected initial v values at small T: a straight line is obtained with a positive slope increasing with v. The same behavior is also found in multiquantum symmetric processes, as for $N_2(v) + N_2(v) \rightarrow N_2(v-w) + N_2(v+w)$ where $w = 2$ and 3 (Fig. 7 and Table S4, ESI†). The efficiency in the symmetric exchange of vibrational quanta of energy decreases as the exchanged number of quanta increases (Fig. 8), but the probability of exchanging a larger number of quanta does not become negligible for higher vibrationally excited states. For the

Table 4 Comparison of V–V rate coefficients calculated with the present PES and those reported in ref. 27 for $N_2(v_1) + N_2(v_2) \rightarrow N_2(v_1') + N_2(v_2')$ transitions

	$v_1, v_2 \rightarrow v_1', v_2'$	200 K	500 K	800 K	1100 K	1400 K	1700 K	2000 K	2900 K
Present	10, 10 → 9, 11	7.80×10^{-13}	1.08×10^{-12}	1.53×10^{-12}	2.04×10^{-12}	2.60×10^{-12}	3.20×10^{-12}	3.81×10^{-12}	5.65×10^{-12}
Ref. 27	10, 10 → 9, 11	1.38×10^{-12}	2.00×10^{-12}	2.84×10^{-12}	3.81×10^{-12}	4.84×10^{-12}	5.87×10^{-12}	6.88×10^{-12}	9.81×10^{-12}
Present	42, 0 → 40, 1	2.35×10^{-14}	2.47×10^{-14}	3.27×10^{-14}	4.19×10^{-14}	5.13×10^{-14}	6.08×10^{-14}	7.03×10^{-14}	1.00×10^{-13}
Ref. 27	42, 0 → 40, 1	4.04×10^{-14}	5.59×10^{-14}	7.65×10^{-14}	9.82×10^{-14}	1.19×10^{-13}	1.36×10^{-13}	1.52×10^{-13}	1.90×10^{-13}

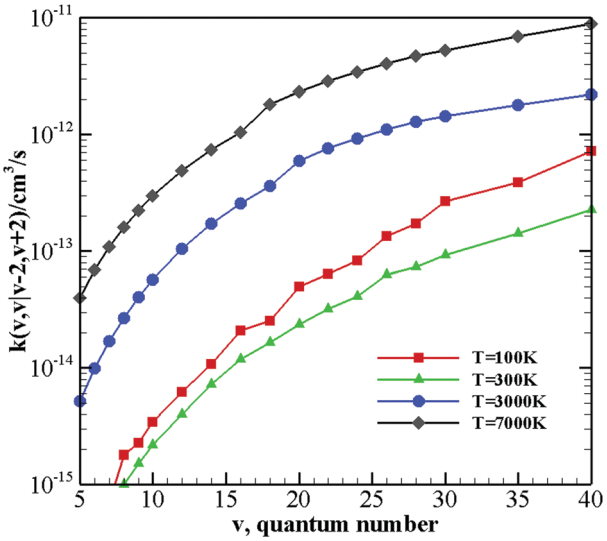

Fig. 7 V–V rate coefficients for $N_2(v) + N_2(v) \rightarrow N_2(v-2) + N_2(v+2)$ processes as a function of the vibrational quantum number v at different temperature values.

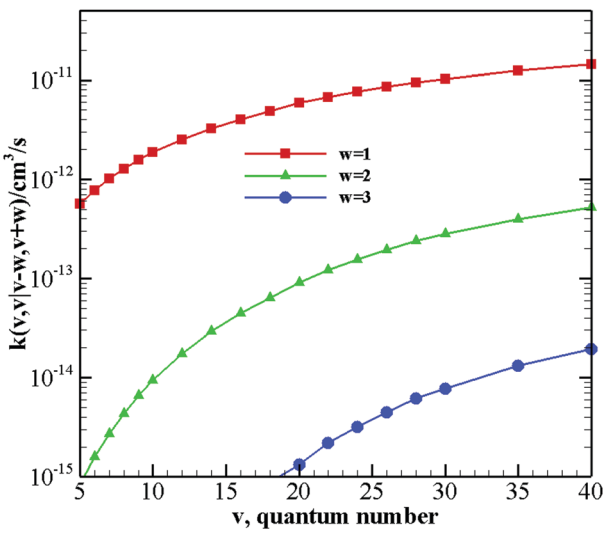

Fig. 8 V–V rate coefficients for $N_2(v) + N_2(v) \rightarrow N_2(v-w) + N_2(v+w)$ processes as a function of the vibrational quantum number v for the exchange of 1, 2 and 3 vibrational quanta of energy at T = 1000 K.

asymmetric multiquantum process $N_2(v) + N_2(0) \rightarrow N_2(v-2) + N_2(1)$ (Fig. 9), the anti-Arrhenius behavior of the rate coefficients is not present, except when nearly resonant transitions are considered. Furthermore, many of these processes turn out to be quite efficient (though, as mentioned before, some caution is needed when taking their absolute value), with rate coefficients comparable or larger than those for symmetric double quantum exchange transitions, thus playing an important role in the kinetic modeling.

V–T/R rate coefficients were determined for processes where vibrational relaxation occurs due to the collision between N_2 in its vibrational ground state and a vibrationally excited molecule,

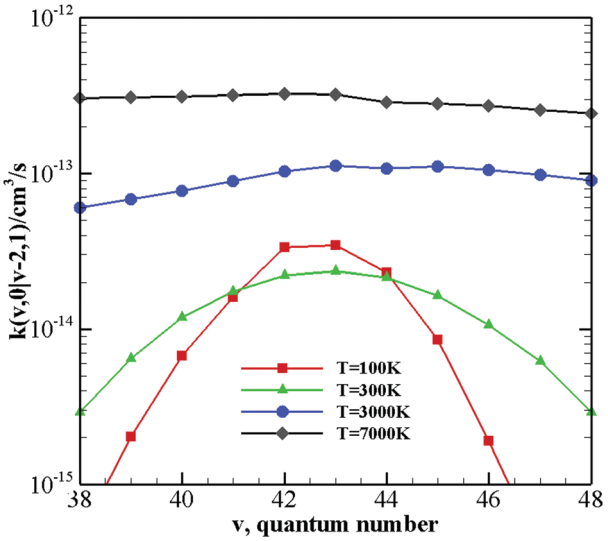

Fig. 9 V–V rate coefficients for $N_2(v) + N_2(0) \rightarrow N_2(v-2) + N_2(1)$ processes as a function of the vibrational quantum number v at different temperature values.

with the loss of a single quantum of vibrational energy (Table S6, ESI†), two vibrational quanta (Table S7, ESI†) or more (Table S8, ESI†). Vibrational relaxation upon collision between two equally vibrationally excited molecules was also considered (Table S9, ESI†).

The results show that, though the rate of V–T/R processes is extremely low at low temperature (being generally some orders of magnitude smaller than V–V processes for the same initial vibrational states, see the following), their efficiency rapidly grows by increasing the temperature, and they become comparable, or, in some cases, even the most efficient events at high temperature values.

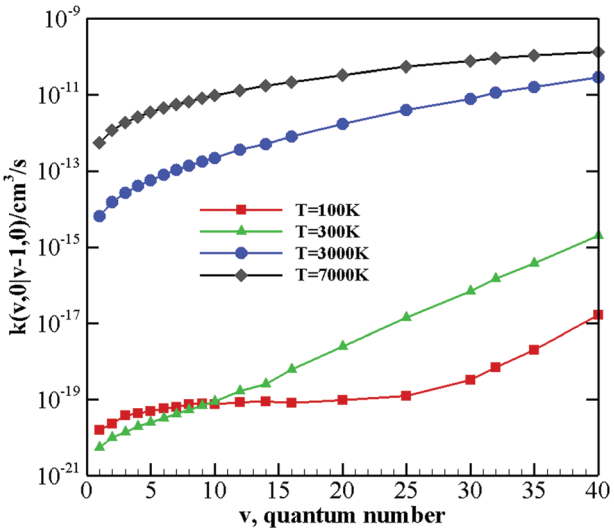

Fig. 10 V–T/R rate coefficients for $N_2(v) + N_2(0) \rightarrow N_2(v-1) + N_2(0)$ processes as a function of the vibrational quantum number v at different temperature values.

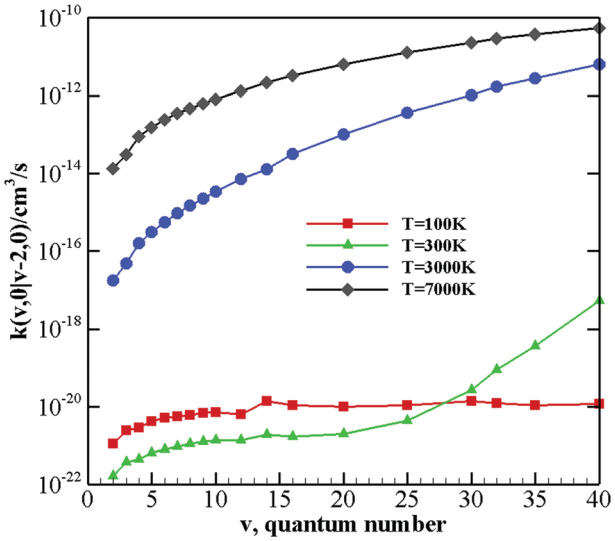

Fig. 11 V–T/R rate coefficients for $N_2(v) + N_2(0) \rightarrow N_2(v-2) + N_2(0)$ processes as a function of the vibrational quantum number v at different temperature values.

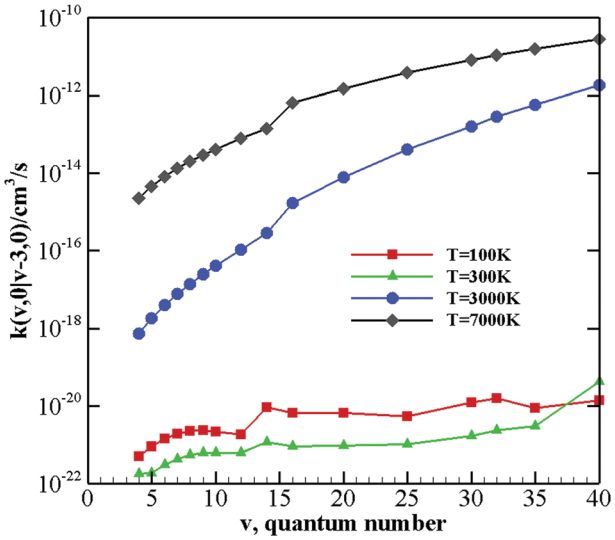

Fig. 12 V–T/R rate coefficients for $N_2(v) + N_2(0) \rightarrow N_2(v-3) + N_2(0)$ processes as a function of the vibrational quantum number v at different temperature values.

The behavior of rate coefficients for V–T/R processes $N_2(v) + N_2(0) \rightarrow N_2(v-w) + N_2(0)$, with $w = 1, 2, 3$, as a function of the initial quantum number v at $T = 100$, 300, 3000, and 7000 K is reported in Fig. 10, 11 and 12 for the various w values, respectively. All the figures, at high temperatures, show a more pronounced increase of vibrational relaxation when increasing the vibrational excitation of the $N_2(v)$ molecule. This enhancement with the initial v value is more evident as the number of lost vibrational quanta w grows.

At low temperature, on the other hand, this behavior seems to be connected to the value of v and to the number of quanta w to be lost. Indeed, at low temperature the rate coefficients for the loss of vibrational quanta remain practically constant until a sufficiently high value of v is reached. It is worth noting that for low vibrational excited states at $T \leq 300$ K many of the rate coefficients have an absolute value smaller than 10^{-20} cm^3 s^{-1}, which is close to the numerical accuracy of the present method, so that such values may not be as accurate as larger ones. However, the very good agreement with the experimental results mentioned in ref. 39 at 300 K (and, to a lesser extent, with those at 500 K mentioned in ref. 38, however an older determination, see Table S1 (ESI†)), suggests that these values can be taken quite confidently. In any case, we believe that the general trend of these processes as a function of temperature and of v might be an important issue. At 100 K the rate of vibrational relaxation remains small (less than 10^{-19} cm^3 s^{-1}, for any v, except in the case of $w = 1$ for $v \geq 25$). The same trend can be found at $T = 300$ K, when two vibrational quanta are lost, with rate coefficients starting to increase for $v \geq 25$ and with three vibrational quanta ($w = 3$) for $v > 35$.

Furthermore, an anti-Arrhenius temperature behavior of the rate coefficients seems again to be present in all $N_2(v) + N_2(0) \rightarrow N_2(v-w) + N_2(0)$ processes for small v values (see Fig. S5 and S6, ESI†); as w increases the value of the vibrational quantum number v needed to restore the increase of the rate coefficients with temperature behavior increases.

Table S9 (ESI†) reports V–T/R rate coefficients for the loss of one or two vibrational quanta of energy when both colliding partners are in the same vibrational excited state, *i.e.* $N_2(v) + N_2(v)$ for $v = 5$, 10, 20, 30 and 40, whereas Fig. 13 shows the behavior of the rate coefficients as a function of temperature for different numbers of lost vibrational quanta. Again a strong increase of the rate coefficients with temperature is observed in all cases, with some processes, particularly those with smaller v values, showing the above mentioned anti-Arrhenius behavior at low T. As expected, the loss of multiple vibrational quanta is a less probable event, and, in the case of the loss of two quanta, the symmetric process, *i.e.* the loss of a single quantum by each of the N_2 diatom, is slightly more probable than the asymmetric one.

It might be interesting, as noted before, to compare the relative efficiency of V–V and V–T/R processes, starting from the well studied collision $N_2(1) + N_2(0)$, depicted in Fig. S3 (ESI†), which shows that the V–V process is by far the favored one up to $T = 5000$ K. Above such temperatures, however, the V–T/R relaxation becomes predominant. The same behavior is found for the symmetric collisions $N_2(v) + N_2(v)$ (Fig. 13).

For the collision between a highly vibrationally excited molecule and $N_2(0)$ such behavior starts at much smaller values of temperature (Fig. 14). Indeed, the loss of one vibrational quantum is the favored process at temperatures above 500 K, and the processes corresponding to the loss of two and three vibrational quanta are far more efficient than V–V processes at $T > 2000$ K.

The results thus indicate that V–T/R processes are competitive with V–V ones and very relevant to the correct modelling of high temperature situations as those occurring in hypersonic flows or plasma or situations of interest in aerospace science, so that accurate databases are needed to extend the existing ones for V–V rate coefficients.

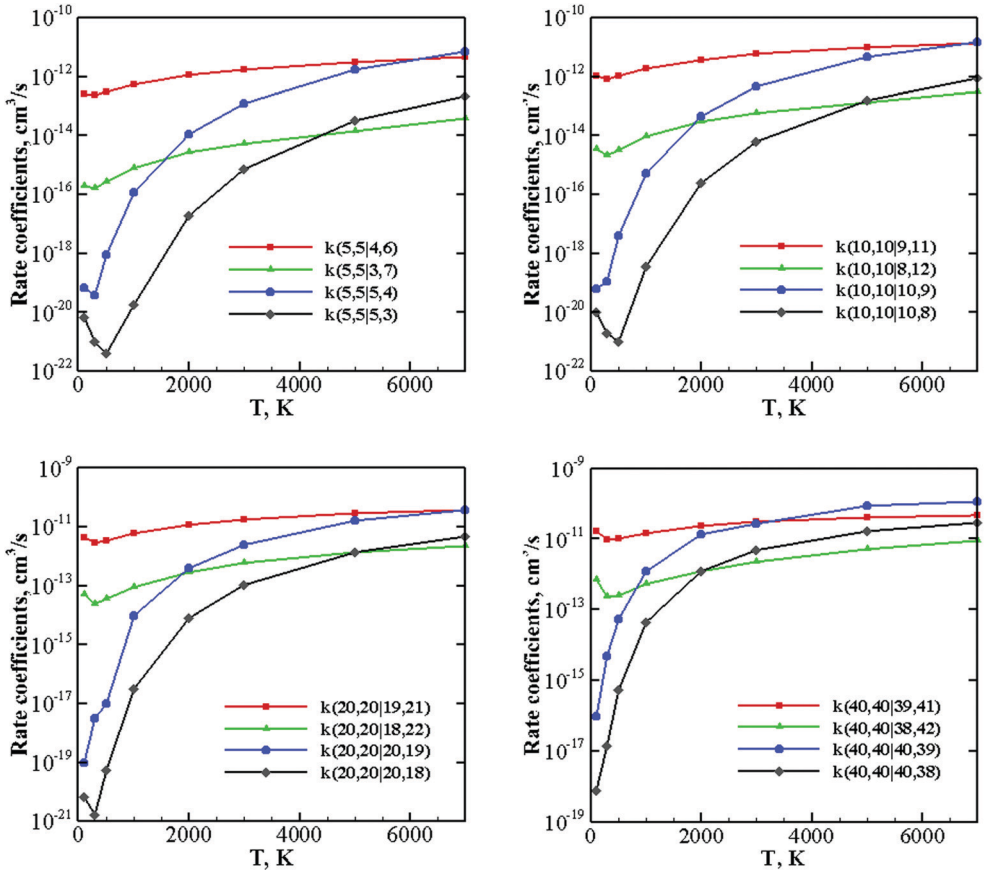

Fig. 13 V–T/R and V–V rate coefficients for some selected $N_2(v)$ + $N_2(v)$ processes as a function of temperature for v = 5, 10, 20 and 40.

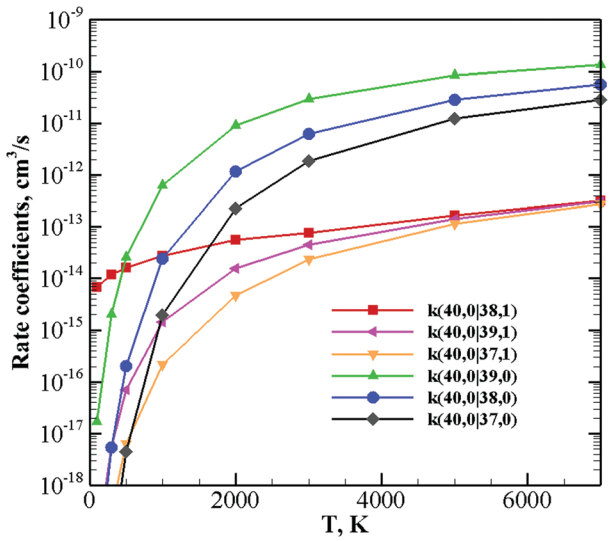

Fig. 14 V–T/R and V–V rate coefficients for selected $N_2(40)$ + $N_2(0)$ processes as a function of temperature.

5 Conclusions

The possibility of modulating the behavior of the analytical potential energy surface, using the improved Lennard-Jones method, where parameters have a strong physical meaning, in a flexible and general way was exploited to improve the accuracy of such potential in a large range of temperatures for the calculation of V–V and V–T/R rate coefficients. From such analysis, closely checked by comparing the behavior of the PES against accurate high level *ab initio* calculations, some physical insights into the stereodynamics of the process could also be assessed, like the fact that collinear collisions are those most affecting the transfer of vibrational quanta of energy in diatom–diatom dynamics. Though the performed modifications were mainly meant to improve the description of the inelastic scattering dynamics in the high temperature regime, mostly important for the modelling of hypersonic flows and aerospace applications, it turns out that they also produce a better behavior of the PES against the calculation of several different properties, ranging from the virial coefficient to quantum interference effects in scattering.

The new potential was then used to produce a large database of V–V rate coefficients (enlarging existing ones) and, above all, of V–T/R coefficients, whose calculation generally represents a much more demanding task from the computational point of view. The use of the quantum-classical method together with an efficient analytical potential makes it possible to perform such a task. The relative magnitude of such coefficients shows the relevant role played by V–T/R processes at high temperatures,

which, in some cases, become by far the most probable events, indicating that they need to be included for an accurate modeling of such conditions.

Besides the limitations of the method in the description of very highly excited vibrational states, the correct treatment under extreme temperature conditions, *i.e.* very low or very high temperature (higher than those considered in the present work) also needs to lift some approximations of the utilized approach. At very low temperatures, rotations should also be included in the quantum subsystem and effects due to the nuclear spins might come into play. At very high temperatures the possibility of populating very high vibrational states and thus of bond breaking and reactivity should be considered in both the potential and in the dynamical treatment.

The present investigation is intended to be the first one of a series where a systematic approach is used to build PESs in an internally coherent fashion, *i.e.* by using a physically meaningful analytical formulation of the potential performing well in wide temperature ranges, tested against *ab initio* calculations and available experimental properties of a different kind, in order to exploit such potentials for the determination of large bodies of inelastic scattering cross sections, involving vibrational energy transfer. Work is in progress to extend such a methodology to other diatom–diatom systems also consisting of molecules of a different type.

Conflicts of interest

There are no conflicts to declare.

Acknowledgements

This work was supported by the Strategic Priority Research Program of Chinese Academy of Sciences (Grant No. XDA17030100) and the National Natural Science Foundation of China through grants 11372325 and 91116013. M. B. acknowledges the FIS2017-84391-C2-2-P Spanish grant for funding.

Notes and references

1 V. Guerra and J. Loureiro, *J. Phys. D: Appl. Phys.*, 1995, **28**, 1903.
2 M. Capitelli, C. M. Ferreira, B. F. Gordiets and A. I. Osipov, *Plasma kinetics in atmospheric gases*, Springer Science & Business Media, 2013, vol. 31.
3 C. Park, *Nonequilibrium hypersonic aerothermodynamics*, Wiley, 1990.
4 I. Armenise and M. Capitelli, *Plasma Sources Sci. Technol.*, 2005, **14**, S9.
5 F. Esposito, *Rendiconti Lincei. Scienze Fisiche e Naturali*, 2019, **30**, 57–66.
6 A. Lagana, E. Garcia and L. Ciccarelli, *J. Phys. Chem.*, 1987, **91**, 312–314.
7 J. D. Bender, P. Valentini, I. Nompelis, Y. Paukku, Z. Varga, D. G. Truhlar, T. Schwartzentruber and G. V. Candler, *J. Chem. Phys.*, 2015, **143**, 054304.
8 E. Garcia, T. Martnez and A. Laganà, *Chem. Phys. Lett.*, 2015, **620**, 103–108.
9 F. Esposito, I. Armenise and M. Capitelli, *Chem. Phys.*, 2006, **331**, 1–8.
10 F. Esposito, E. Garcia and A. Laganá, *Plasma Sources Sci. Technol.*, 2017, **26**, 045005.
11 S. Fioccola, F. Pirani, M. Bartolomei and C. Coletti, *International Conference on Computational Science and Its Applications*, 2017, pp. 281–296.
12 A. Kurnosov, M. Cacciatore, A. Laganà, F. Pirani, M. Bartolomei and E. Garcia, *J. Comput. Chem.*, 2014, **35**, 722–736.
13 A. Lombardi, F. Pirani, M. Bartolomei, C. Coletti and A. Laganà, *Front. Chem.*, 2019, **7**, 309.
14 C. Coletti and G. D. Billing, *J. Chem. Phys.*, 2000, **113**, 4869–4875.
15 G. D. Billing and M. Cacciatore, *Chem. Phys. Lett.*, 1983, **94**, 218–221.
16 D. Cappelletti, F. Pirani, B. Bussery-Honvault, L. Gomez and M. Bartolomei, *Phys. Chem. Chem. Phys.*, 2008, **10**, 4281–4293.
17 M. Cacciatore, A. Kurnosov and A. Napartovich, *J. Chem. Phys.*, 2005, **123**, 174315.
18 M. H. K. Jafari, A. Maghari and S. Shahbazian, *Chem. Phys.*, 2005, **314**, 249–262.
19 R. Hellmann, *Mol. Phys.*, 2013, **111**, 387–401.
20 Y. Paukku, K. R. Yang, Z. Varga and D. G. Truhlar, *J. Chem. Phys.*, 2013, **139**, 044309.
21 L. Gomez, B. Bussery-Honvault, T. Cauchy, M. Bartolomei, D. Cappelletti and F. Pirani, *Chem. Phys. Lett.*, 2007, **445**, 99–107.
22 G. Billing, *Comput. Phys. Commun.*, 1984, **32**, 45–62.
23 G. Billing, *Comput. Phys. Commun.*, 1987, **44**, 121–136.
24 D. Babikov and A. Semenov, *J. Phys. Chem. A*, 2016, **120**, 319–331.
25 B. Mandal, D. Babikov and A. Semenov, *J. Phys. Chem. A*, 2018, **122**, 6157–6165.
26 C. Coletti and G. D. Billing, *J. Chem. Phys.*, 1999, **111**, 3891–3897.
27 A. Kurnosov, A. Napartovich, S. Shnyrev and M. Cacciatore, *Plasma Sources Sci. Technol.*, 2010, **19**, 045015.
28 G. Billing, *Comput. Phys. Rep.*, 1984, **1**, 237–296.
29 R. Hamming, *Numerical methods for scientists and engineers*, Dover Publications, New York, 1986.
30 K. Huber and G. Herzberg, *The Theory of Rotating Diatomic Molecules*, 1975.
31 F. Pirani, S. Brizi, L. F. Roncaratti, P. Casavecchia, D. Cappelletti and F. Vecchiocattivi, *Phys. Chem. Chem. Phys.*, 2008, **10**, 5489–5503.
32 F. Pirani, M. Albert, A. Castro, M. M. Teixidor and D. Cappelletti, *Chem. Phys. Lett.*, 2004, **394**, 37–44.
33 C. Douketis, G. Scoles, S. Marchetti, M. Zen and A. Thakkar, *J. Chem. Phys.*, 1982, **76**, 3057–3063.
34 R. Candori, F. Pirani and F. Vecchiocattivi, *Chem. Phys. Lett.*, 1983, **102**, 412–415.
35 M. Bartolomei, E. Carmona-Novillo, M. I. Hernandez, J. Campos-Martinez and R. Hernandez-Lamoneda, *J. Comput. Chem.*, 2011, **32**, 279–290.
36 A. Lombardi, F. Pirani, A. Laganà and M. Bartolomei, *J. Comput. Chem.*, 2016, **37**, 1463–1475.
37 R. C. Millikan and D. R. White, *J. Chem. Phys.*, 1963, **39**, 3209–3213.

38 M. C. Henderson, *J. Acoust. Soc. Am.*, 1962, **34**, 349–350.
39 M. Chatelet and J. Chesnoy, *Chem. Phys. Lett.*, 1985, **122**, 550–552.
40 T. Ahn, I. V. Adamovich and W. R. Lempert, *Chem. Phys.*, 2004, **298**, 233–240.
41 S. Valyanskii, K. Vereshchagin, A. Volkov, P. Pashinin, V. Smirnov, V. Fabelinskii and L. Holz, *Quantum Electron.*, 1984, **14**, 1229.
42 R. Z. Martnez and D. Bermejo, *Phys. Chem. Chem. Phys.*, 2015, **17**, 12661–12672.
43 Y. S. Akishev, A. Demyanov, I. Kochetov, A. Napartovich, S. Pashkin, V. Ponomarenko, V. Pevgov and V. Podobedov, *High Temp.*, 1982, **20**, 658.
44 R. A. Kendall, J. T. H. Dunning and R. J. Harrison, *J. Chem. Phys.*, 1992, **96**, 6796.
45 F. Tao and Y. K. Pan, *J. Chem. Phys.*, 1992, **97**, 4989.
46 S. F. Boys and F. Bernardi, *Mol. Phys.*, 1970, **19**, 553.
47 H.-J. Werner, P. J. Knowles, F. R. Knizia, G. Manby and M. Schütz, *A Package of Ab initio Programs. Molpro, Version*, 2012.
48 V. Aquilanti, M. Bartolomei, D. Cappelletti, E. Carmona-Novillo and F. Pirani, *J. Chem. Phys.*, 2002, **117**, 615–627.
49 R. T. Pack, *Chem. Phys. Lett.*, 1978, **55**, 197–201.
50 M. Ewing and J. Trusler, *Phys. A*, 1992, **184**, 415–436.
51 T. N. Olney, N. Cann, G. Cooper and C. Brion, *Chem. Phys.*, 1997, **223**, 59–98.